Neurobiology of Disease

Robust Pacemaking in Substantia Nigra Dopaminergic Neurons

Jaime N. Guzman,* Javier Sánchez-Padilla,* C. Savio Chan, and D. James Surmeier
Department of Physiology, Feinberg School of Medicine, Northwestern University, Chicago, Illinois 60611

Dopaminergic neurons of the substantia nigra pars compacta are autonomous pacemakers. This activity is responsible for the sustained release of dopamine necessary for the proper functioning of target structures, such as the striatum. Somatodendritic L-type Ca^{2+} channels have long been viewed as important, if not necessary, for this activity. The studies reported here challenge this viewpoint. Using a combination of optical and electrophysiological approaches in brain slices, it was found that antagonism of L-type Ca^{2+} channel effectively stopped dendritic Ca^{2+} oscillations but left autonomous pacemaking unchanged. Moreover, damping intracellular Ca^{2+} oscillations with exogenous buffer had little effect on pacemaking rate. Although not necessary for pacemaking, L-type channels helped support pacemaking when challenged with cationic channel blockers. Simulations suggested that the insensitivity to antagonism of L-type channels reflected the multichannel nature of the pacemaking process. The robustness of pacemaking underscores its biological importance and provides a framework for understanding how therapeutics targeting L-type Ca^{2+} channels might protect dopaminergic neurons in Parkinson's disease without compromising their function.

Introduction

Dopamine (DA)-releasing neurons of the substantia nigra pars compacta (SNc) are critical to a broad array of psychomotor functions, including action selection and reward-based learning (Schultz, 2007; Yin et al., 2008; Cohen and Frank, 2009). A key feature of these neurons is their steady, autonomous pacemaking. This self-generated activity maintains extracellular DA levels and the DA receptor signaling necessary for normal network operation in basal ganglia structures, such as the striatum (Albin et al., 1989; Gonon and Bloch, 1998). Although synaptic signals are capable of altering ongoing spike activity *in vivo* (Grace and Bunney, 1984; Tepper et al., 1998), the rate and regularity of the autonomous activity is remarkably robust in the face of a variety of pharmacological and molecular perturbations (Paladini et al., 2003; Chan et al., 2007).

The mechanisms underlying autonomous pacemaking have been the subject of investigation for more than a decade. At present, the dominant view is that, in adult SNc dopaminergic neurons, pacemaking is dependent on Ca^{2+} channels that open at relatively hyperpolarized membrane potentials (Nedergaard et al., 1993; Mercuri et al., 1994; Amini et al., 1999; Wilson and Callaway, 2000; Puopolo et al., 2007). Based on the ability of dihydropyridines (DHPs) to slow or stop pacemaking, this channel has been assumed to be of the Ca_v1 or L-type (Nedergaard et al., 1993; Mercuri et al., 1994; Chan et al., 2007; Puopolo et al., 2007). However, the DHP concentrations necessary to achieve significant slowing or silencing in these acute physiological experiments are typically several orders of magnitude greater than those predicted by binding studies to be required for near complete channel antagonism (Koschak et al., 2001; Sinnegger-Brauns et al., 2009). In principle, there are several factors that might contribute to this mismatch. For example, the affinity of DHPs for L-type channels is state dependent, being approximately a thousand-fold lower at negative membrane potentials (Bean, 1984). Another major limitation is the difficulty in achieving binding equilibrium in brain slices. Lipophilic DHPs not only must diffuse tens of micrometers into the slice, they must partition into the membrane and diffuse to a binding site buried in the lipid bilayer (Lipkind and Fozzard, 2003). This makes equilibrium slow to achieve, taking as much as an hour (Herbette et al., 1989). Because electrophysiological recordings are typically stable for a much shorter period of time, high DHP concentrations have been used to achieve measurable levels of channel antagonism rapidly. This approach has a number of caveats, not the least of which is that, because DHPs have very high membrane partition coefficients (Herbette et al., 1989), their concentration can reach levels that begin to have nonspecific effects on other ion channels, complicating the interpretation of effects on complex phenomena, such as pacemaking.

Determining the role of L-type Ca^{2+} channels in pacemaking is not only of theoretical importance but of clinical importance as well. Ca^{2+} ions entering SNc DA neurons through L-type Ca^{2+} channels during pacemaking elevates cellular vulnerability to toxins used to create animal models of Parkinson's disease (PD) (Chan et al., 2007). The potential linkage of these channels to PD has been strengthened by epidemiological studies showing a decreased disease risk in humans treated for hypertension with

Received May 30, 2009; revised July 13, 2009; accepted July 27, 2009.

This work was supported by the Hartman Foundation, the Falk Trust, United States Army Medical Research and Material Command Grant W81 XWH-071-0170, and National Institutes of Health Grant NS047085. We thank Karen Saporito, Sasha Ulrich, David Wokosin, and Ema Ilijic for their technical support and scientific contributions.

*J.N.G. and J.S.-P. contributed equally to this work.

Correspondence should be addressed to Dr. D. James Surmeier, Department of Physiology, Feinberg School of Medicine, Northwestern University, 303 East Chicago Avenue, Chicago, IL 60611. E-mail: j-surmeier@northwestern.edu.

DOI:10.1523/JNEUROSCI.2519-09.2009

 0270-6474/09/2911011-09$15.00/0

DHPs (Becker et al., 2008). However, if L-type channels are critical to pacemaking, this therapeutic benefit must come at a functional cost, such as a drop in pacemaking rate and DA in target structures. Using optical and electrophysiological approaches to assay acute L-type channel antagonism, we show that, although these channels contribute to the robustness of pacemaking, they are not necessary.

Materials and Methods

Electrophysiological recordings. Acute midbrain coronal slices (220 μm thick) were obtained from wild-type male C57BL/6 mice (Charles River) between postnatal ages 21 and 32 d, unless specified otherwise. The handling of mice and all procedures performed on them were approved by the institutional Animal Care and Use Committee and were in accordance with the National Institutes of Health *Guide to the Care and Use of Laboratory Animals* and Society for Neuroscience guidelines. Mice were anesthetized with a ketamine/xylazine mixture, followed by a transcardial perfusion with ice-cold, oxygenated artificial CSF (ACSF) containing the following (in mM): 125 NaCl, 2.5 KCl, 25 $NaHCO_3$, 1.25 NaH_2PO_4, 2 $CaCl_2$, 1 $MgCl_2$, and 25 dextrose, pH 7.3 (osmolality 315–320 mOsm/L). After perfusion, mice were decapitated and brains were removed rapidly, followed by sectioning in ice-cold oxygenated ACSF using a vibratome (VT1000S; Leica Microsystems). Midbrain slices recovered in ACSF at 34°C for 30 min before electrophysiological recordings. Slices were transferred to a small-volume (<0.5 ml) recording chamber that was mounted on a fixed-stage, upright microscope (BX51; Olympus America) equipped with infrared differential interference contrast [0.9 numerical aperture (NA)] with de Sénarmont compensation (Olympus). Experiments were performed at 33–34°C, unless specified otherwise. The recording chamber was superfused with carbogen-saturated ACSF with a flow rate of 2–3 ml/min running through an in-line heater (SH-27B with TC-324B controller; Warner Instruments). Neuronal somata and proximal dendrites were visualized by video microscopy at high magnification (60×, 0.9 NA water-immersion objective; Olympus). Cell-attached and whole-cell patch-clamp recordings were performed in DA neurons from the mid-to-ventral tier of the SNc. Recording patch electrodes (resistance of 3–4 MΩ) were prepared with a Sutter Instruments horizontal puller using borosilicate glass with filament. For all voltage- and current-clamp recordings, patch electrodes were filled with internal solution containing the following (in mM): 135 K-$MeSO_4$, 5 KCl, 5 HEPES, 0.05 EGTA, 10 phosphocreatine-di(tris), 2 ATP-Mg, and 0.5 GTP-Na, the pH adjusted to 7.3 (osmolality adjusted to 290–300 mOsm/L). The liquid junction potential in our recording ACSF was 7 mV and not corrected for. Conventional tight-seal (>3 GΩ) whole-cell patch-clamp and cell-attached recordings were made on visually identified neurons based on (1) size and somatodendritic morphology, (2) regular spiking between 1 and 4 Hz, (3) presence of a voltage sag during delivery of a hyperpolarizing pulse (−250 pA current injection), and (4) the presence of the HCN current recorded in voltage clamp (data not shown). For Na^+ current recordings, voltage control and space clamp was improved by lowering the external concentration of Na^+ to 20 mM and adding 50 μM Cd^{2+} to the perfusate; patch electrodes were filled with a cesium-based internal containing the following (in mM): 120 Cs-$MeSO_3$, 15 CsCl, 8 NaCl, 10 HEPES, 0.2 EGTA, 3 ATP-Mg, 0.3 GTP-Na, and 10 tetraethylammonium-Cl, pH 7.3 (osmolality 280 mOsm/L). Tetrodotoxin (TTX)-sensitive sodium currents were recorded in voltage clamp with ramps from −70 to −40 mV for 500 ms (ramp speed of 0.06 mV/ms), and peak currents were measured. Signals were filtered at 1–4 kHz and digitized at 5–20 kHz with a Digidata 1322A (Molecular Devices). For current-clamp recordings, the amplifier bridge circuit was adjusted to compensate for electrode resistance and monitored. Electrode capacitance was also compensated. If series resistance increased >20% during recording, the data were discarded.

Two-photon laser scanning microscopy. For dendritic Ca^{2+} measurements, SNc DA neurons in tissue slices (as described above) were loaded with Alexa Fluor 594 (50 μM) and Fluo-4 (200 μM) through the patch pipette. All experiments were performed at 32–34°C. Images were acquired with a 60×/0.9 NA water-immersion lens. Dyes were allowed to equilibrate for at least 15 min before imaging. The two-photon excitation source was a Chameleon-ultra2 tunable laser system (680 to 1080 nm) using titanium:sapphire gain medium with all-solid-state active components and a computer-optimized algorithm to ensure reproducible excitation wavelength, average power, and peak power (Coherent Laser Group). Optical signals were acquired using 810 nm excitation beam (80-MHz pulse repetition frequency and ~250 fs pulse duration) to simultaneously excite Alexa and Fluor-4 dyes. Laser power attenuation was achieved with two Pockel cell electro-optic modulators (models 350-80; Con Optics). The two cells are aligned in series to provide enhanced modulation range for fine control of the excitation dose (0.1% steps over four decades). The laser-scanned images were acquired with a Bio-Rad Radiance MPD system. The fluorescence emission was collected by external or non-descanned photomultiplier tubes (PMTs). The green fluorescence (500–550 nm) was detected by a bialkali-cathode PMT, and the red fluorescence (580–640 nm) was collected by a multi-alkali-cathode (S-20) PMT. The system digitizes the current from detected photons to 12 bits. The laser light transmitted through the sample was collected by the condenser lens and sent to another PMT to provide a bright-field transmission image in registration with the fluorescent images. Measurements were taken in a sample plane along dendritic segments (100–150 mm from the soma). Line scan signals were acquired (as described above) at 6 ms per line and 512 pixels per line with 0.18 μm pixels and 10 μs pixel dwell time. The time between the control and isradipine treatment measurements was 5–7 min.

Statistical analysis. Electrophysiological data collected were analyzed using ClampFit 10.1 (Molecular Devices), Igor Pro 6.0 (Wavemetrics), or Matlab (MathWorks). The stimulation, display, and analysis software for the two-photon imaging data was analyzed using a custom-written shareware package, WinFluor, PicViewer, and PowerCAL kindly provided by John Dempster (Strathclyde University, Glasgow, UK). Data were summarized either using box plots for small sample sizes or with parametric statistics (mean ± SE) for larger samples. Statistical analysis was done with SigmaStat 3.5 (Systat Software) using nonparametric testing Mann–Whitney rank sum test for comparing between two groups or Kruskal–Wallis ANOVA with Dunnett's *post hoc* for multiple group comparison. Before–after statistical analyses were performed using the Wilcoxon's signed rank test. Probability threshold for statistical significance was $p < 0.05$.

Pharmacological reagents and channel ligands. Reagents were purchased from Sigma, except K-$MeSO_4$ (MP Biomedicals), GTP-Na (Roche Diagnostics), isradipine, ZD 7288 (4-ethylphenylamino-1,2-dimethyl-6-methylaminopyrimidinium chloride) (Tocris Bioscience), tetrodotoxin and α-dendrotoxin (Alomone Labs), and BAPTA tetrasodium salt, Alexa594, Fura-2, and Fluo-4 (Invitrogen). Drugs stocks solutions were prepared in deionized water, DMSO, or methanol; on the day of experiment, stocks were diluted to final concentrations in ACSF to achieve a final solvent concentration of <0.01% v/v.

Modeling. Simulations were performed with NEURON, version 5.9 (Hines and Carnevale, 2001). The model neuron was constructed of a cylindrical soma (lateral, 15 μm; dorsal, 15 μm) with axial resistivity of 70 Ω/cm and membrane capacitance of 1 μF/cm^2; the temperature was 35°C, and all conductances had Q_{10} values of 3–4. The density of the simulated channels (siemens per square centimeter) inserted into the membrane were as follows: Na_v1 (3.5e-2), K_v1 (3e-5), K_v2 (2.5e-3), K_v4_{fast} (8.5e-5), K_v4_{slow} (2e-5), K_v7 (7e-7), BK (1e-3), SK (1e-5), HCN (1.25e-4), $Ca_v1.3$ (5e-5), Ca_v2 (1e-5), and leak (3.5e-6); $E_{na} = 50$ mV, $E_k = -90$ mV, and $E_{leak/HCN} = -20$ mV. Kinetics and voltage dependence of channel gating were adjusted to fit experimentally derived values in either SNc DA neurons or other basal ganglia neurons (Mercer et al., 2007); densities were adjusted to fit experimental results and to achieve pacemaking in a normal range. Mod files for Ca^{2+} diffusion, buffering, and pumping were adapted to fit the kinetics observed experimentally using Fluo-4. All of the NEURON mod files used in simulation will be posted on the NeuronDB website (http://senselab.med.yale.edu/neurondb) or are available on request.

Simulations of the modulated DHP receptor were performed with Matlab using the framework proposed by Bean (1984). The channel was assumed to have two affinity states: a high-affinity state at depolarized (inactivated) membrane potentials and a low-affinity state at hyperpo-

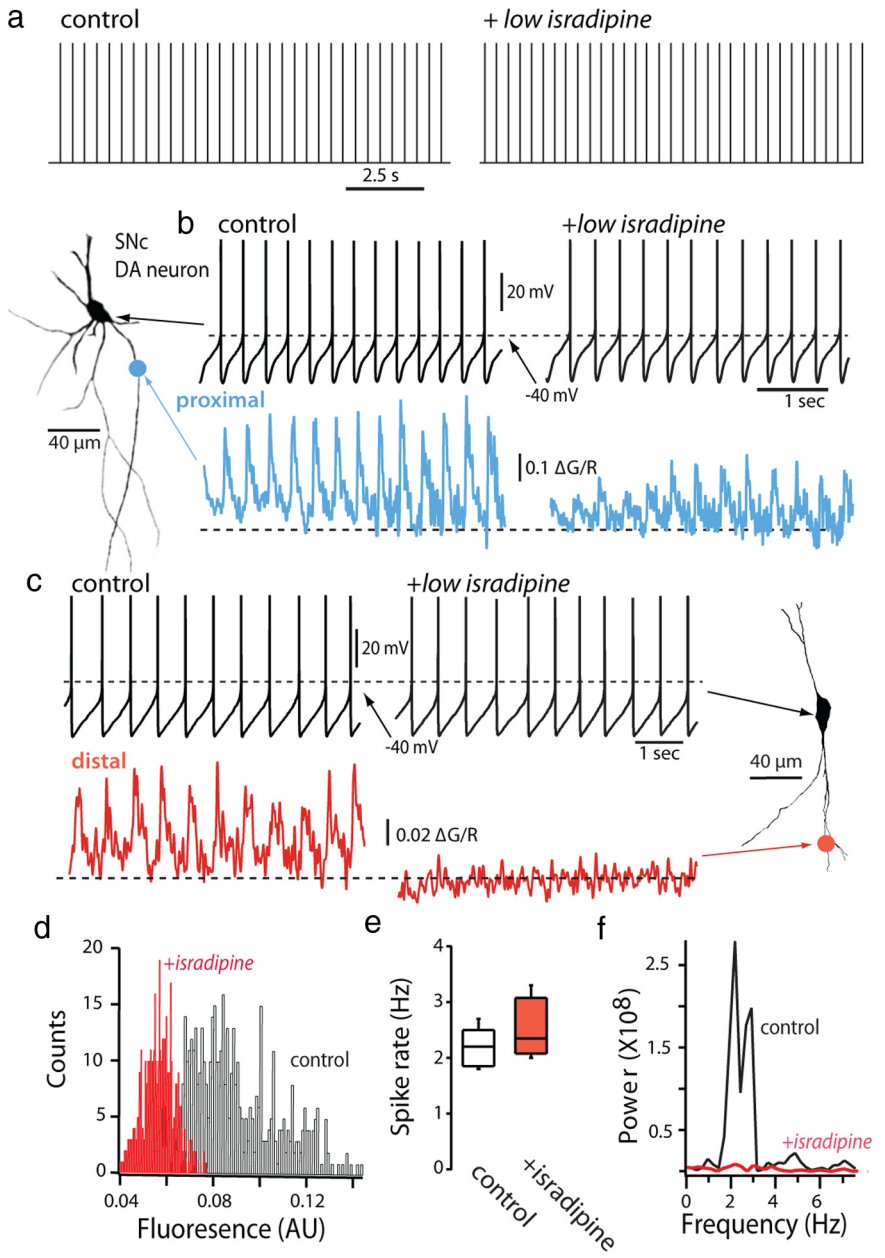

Figure 1. Low concentrations of DHPs suppress dendritic Ca^{2+} oscillations but do not slow pacemaking. ***a***, Digitized cell-attached patch recordings from an SNc DA neuron before and after application of isradipine (5 μM). The median discharge rate before isradipine application was 2.2 and 2.4 Hz after ($p > 0.05$; $n = 10$). ***b***, Whole-cell recording from the cell shown to the left (projection image) before and after isradipine (5 μM) application; there was no significant change in discharge rate in this cell or in 10 others. At the bottom, two-photon laser scanning microscopy measurements of Fluo-4 fluorescence (G) at a proximal dendritic location (~40 μm from the soma) normalized by the fluorescence of the red Alexa dye used to image the cell. ***c***, Somatic recording during imaging at a more distal dendritic location (~120–200 μm from the soma). Note the complete elimination of the spike-associated dendritic Ca^{2+} transient at the distal imaging site. Similar results were obtained in six other neurons. ***d***, All points histogram of fluorescence at the distal location of the cell in ***c*** showing that the median fluorescence was reduced by isradipine. Similar results were obtained in six cells. AU, Arbitrary units. ***e***, Summary showing that, in whole-cell recordings in which imaging was done, isradipine did not change the discharge rate ($p > 0.05$; $n = 10$). ***f***, Spectral analysis of the fluorescence signal readily detected oscillations at the pacemaking frequency; power at this frequency was eliminated by isradipine. Similar results were obtained in six cells.

larized (resting) membrane potentials. The dissociation constant for high-affinity state was assumed to be equal to that found in equilibrium binding studies, whereas the dissociation constant for low-affinity state was assumed to be a thousand-fold higher (Bean, 1984). The macroscopic balance between these states was assumed to be governed by voltage-dependent inactivation of the channel (Bean, 1984); the relationship between steady-state inactivation and voltage for $Ca_v1.3$ channels was taken from the work of Koschak et al. (2001).

Results

Selective antagonism of L-type Ca^{2+} channels does not slow or stop pacemaking

To speed drug delivery to cells buried (30–75 μm below the surface) in a slice, 5 μM isradipine was applied, a concentrations 25–50 times that calculated to achieve near complete blockade of $Ca_v1.3$ channels at the depolarized membrane potentials traversed by SNc DA neurons (Bean, 1984). In cell-attached patch recordings (to minimize rundown), application of 5 μM isradipine for 10 min failed to slow pacemaking (Fig. 1*a*,*b*). This was not because isradipine had not antagonized L-type Ca^{2+} channels. The antagonism could be clearly seen in whole-cell recordings of SNc DA neurons in which oscillations in dendritic Ca^{2+} concentration were monitored using the Ca^{2+} dye Fluo-4 (200 μM). In proximal dendrites (less than ~70 μm from the soma), isradipine clearly reduced the oscillations in Ca^{2+} concentration (Fig. 1*b*). In the more distal (>80 μm from the soma) dendrites, 5 μM isradipine at this time point eliminated any detectable oscillation in Ca^{2+} concentration and lowered modal fluorescence (Fig. 1*c*,*d*). Again, at the time point at which these measurements were made, there was no change in spike rate (Fig. 1*e*). Spectral analysis of the fluorescence signal in these distal dendrites consistently failed to detect power at the pacemaking frequency (Fig. 1*f*).

Another observation that has been taken as evidence of the centrality of L-type channels in pacemaking is that, after block of voltage-dependent Na^+ channels with TTX, the membrane potential continues to oscillate at near the pacemaking frequency (Yung et al., 1991; Nedergaard et al., 1993). These slow oscillatory potentials (SOPs) are widely held to drive pacemaking and trigger Na^+ spikes. However, like the oscillations in dendritic Ca^{2+} concentration, the SOPs were eliminated by application of low micromolar concentrations of isradipine (Fig. 2*a*), concentrations that did not change pacemaking rate when Na^+ channels were left unblocked (Fig. 1*a*). To better test the inferences drawn above, slices were incubated in 200 nM isradipine for 60 min and then patched. If the rate-limiting step in DHP antagonism is diffusion within the lipid bilayer, then at this time point the number of bound channels should be within 10% of the equilibrium value (Herbette et al., 1989); assuming a modal membrane potential of −60 mV (a

conservative estimate), >90% of the $Ca_v1.3$ channels should be antagonized at this point. As predicted from the work with exposure to higher isradipine concentrations, there was no detectable change in pacemaking rate or regularity of SNc DA neurons sampled with cell-attached recordings from slices treated in this way (Fig. 2*b*,*d*). However, invariably, these cells lacked TTX-insensitive SOPs (Fig. 2*c*), arguing that $Ca_v1.3$ Ca^{2+} channels were effectively antagonized. Spectral analysis of the membrane potential in these cells occasionally detected some residual power near the pacemaking rate with exposure to 200 nM isradipine but never with higher concentrations (Fig. 2*e*).

The SOPs seen in the presence of TTX reflect the interplay between dendritic L-type Ca^{2+} channels and small conductance, Ca^{2+}-activated K^+ (SK) channels (Ping and Shepard, 1996; Wilson and Callaway, 2000). If this interplay was necessary for pacemaking, then disrupting the efficient activation of SK channels by chelating intracellular Ca^{2+} should suppress pacemaking. However, whole-cell dialysis with BAPTA (5 mM) did not disrupt pacemaking but rather led to a slow acceleration of pacemaking (Fig. 3*a*), despite its elimination of the SOP seen in the presence of TTX (Fig. 2*b*) and its predicted effect on the trajectory of the spike afterhyperpolarization (Fig. 3*c*). Finally, the temporal properties of the SOPs, which clearly depend on L-type channels, were not consistent with a causal role in pacemaking. First, the frequency of spiking during pacemaking was not strongly correlated with the SOP frequency in the same cell after TTX application (Fig. 3*d*). Second, the coefficient of variation in interval duration during spiking was an order of magnitude smaller than that of the SOP (median CV spiking, 1.9e-4; median CV oscillation, 3.2e-2; $n = 9$; $p < 0.05$), and examination of successive intervals consistently showed random scatter in the SOP interval, even when the interspike interval in the same cell was very regular (Fig. 3*e*).

The insensitivity of pacemaking to DHPs seen in our work differs from that seen in younger, acutely isolated SNc DA neurons from mice (Puopolo et al., 2007). One possible explanation is that the work with acutely isolated neurons was performed at room temperature, some 10°C cooler than the experiments described here. To test this hypothesis, SNc DA neurons in slices were recorded at 23–25°C. At this temperature, pacemaking rate in cell-attached recordings was ap-

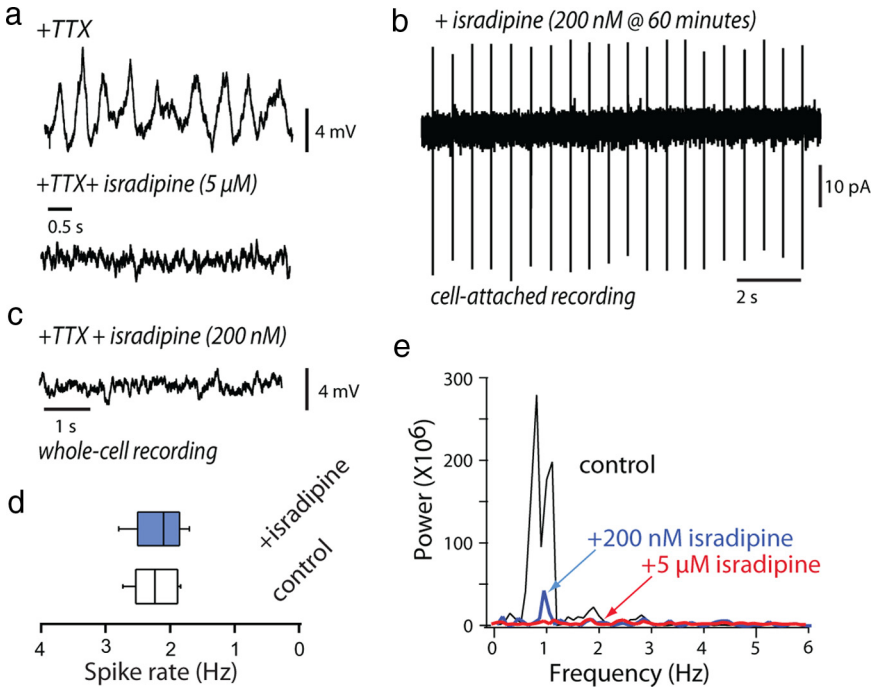

Figure 2. Submicromolar levels of DHPs are sufficient to block SOPs without compromising pacemaking activity. ***a***, Representative SOP traces (after blockade of sodium channels with 1 μM TTX) in the presence or absence of isradipine (5 μM). Micromolar concentrations of isradipine (5 μM) blocked the TTX-insensitive SOPs ($n = 10$ cells). ***b***, Submicromolar concentrations of DHPs (200 nM isradipine) had no effect in pacemaking firing rate ($p > 0.05$; $n = 5$ cells). ***c***, Representative current-clamp trace showing no SOPs of a DA neuron pretreated with 200 nM isradipine for 1 h ($n = 5$ cells). ***d***, Summary box plots showing that 200 nM isradipine had no effect in spike rate. ***e***, Spectral analysis of the fluorescence showing a significant reduction in the power of the frequency detected in control, highly reduced power in the presence of 200 nM isradipine and complete elimination of frequency by 5 μM isradipine.

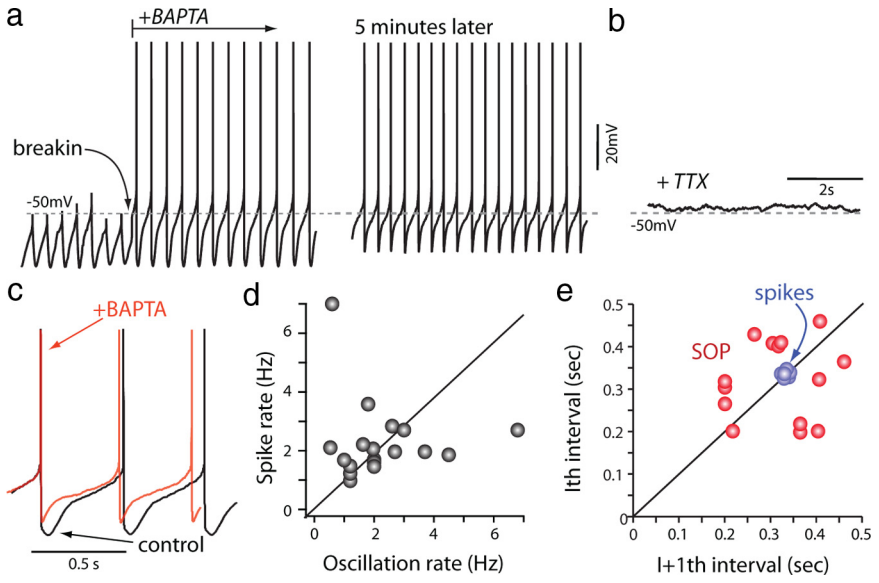

Figure 3. SOPs are absent after chelation of intracellular calcium. ***a***, Recording from an SNc DA neuron with an electrode containing 5 mM BAPTA. Before break-in, the pacemaking rate could be seen; after break-in, the rate slowly increased and the afterhyperpolarization became less pronounced, as shown in ***d***. Similar results were obtained in six cells. ***b***, Application of TTX demonstrated the absence of SOPs in the presence of BAPTA. ($n = 4$). ***c***, Voltage traces from ***b*** early (black trace) and later (red trace) in the dialysis with BAPTA showing the change in the afterhyperpolarization. ***d***, The discharge rate before application of TTX is plotted against the frequency of SOP oscillation. Note the scatter around the line with a slope of 1 ($n = 19$). ***e***, Plots of successive spike intervals or successive SOP intervals (measured from the point at which the voltage reached the median voltage of the oscillation). A sample of nine cells is plotted. Note the tight clustering of the spike data and the dispersion of the SOP data.

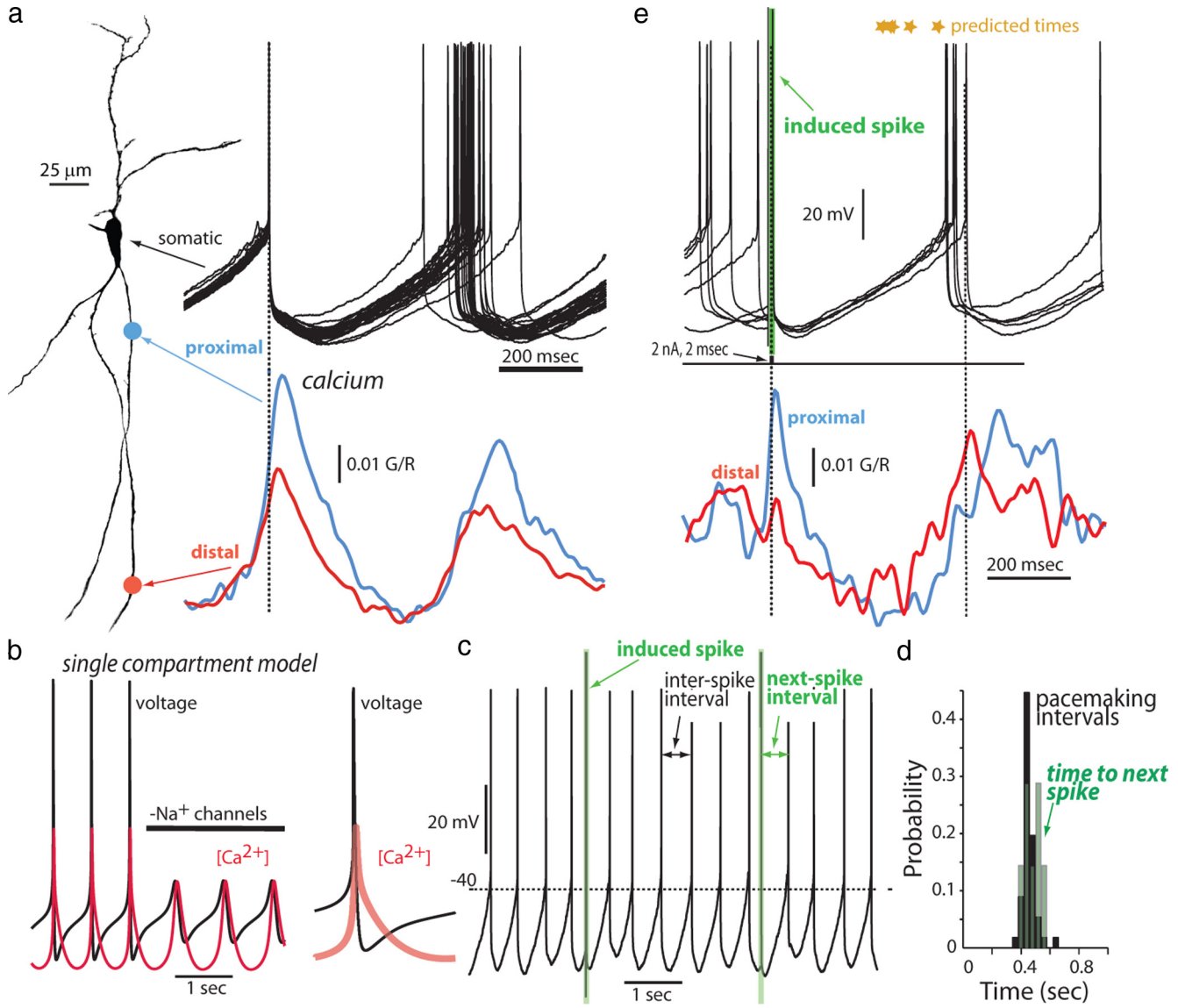

Figure 4. Dendritic Ca^{2+} oscillations are phase locked to somatic spiking. ***a***, Projection image of an SNc DA neuron recorded from with a somatic patch electrode containing Alexa 594 (50 μM) and the Ca^{2+} dye Fluo-4 (200 μM). To the right are somatic voltage recordings during pacemaking. At the bottom are averages of the fluorescence changes (G/R) at two dendritic locations shown by blue (proximal) and red (distal) dots. The averages were computed by aligning segments of the fluorescence records of 10 successive spikes; because the timing of the next spike varied, the timing of the fluorescence change after the initial spike in the average is only approximate and was used to gauge the phase relationship of the Ca^{2+} oscillation. ***b***, A simulation using a single compartment model showing the relationship between the voltage (black trace) and the rise in intracellular Ca^{2+} concentration (red) before and after block of Na^{+} channels; note the similarity between these records and the data in ***a*** where Ca^{2+} concentration rises just before the spike and peaks after the spike, falling during the afterhyperpolarization. ***c***, Recording from an SNc DA neuron in which ectopic spikes were introduced by brief (2 ms) current pulses; the green bar shows the timing of the ectopic spikes. ***d***, Histogram of the intervals during normal pacemaking (black filled) and the intervals after an ectopic spike (green filled) showing that it generated an interval typical of normal pacemaking, regardless of its phase relationship to the ongoing spiking. Similar behavior was seen in all four cells examined in this way. ***e***, At the top, somatic voltage records from one of these experiments showing the ectopic spike; at the bottom, fluorescence records (G/R) at the same locations shown in ***a***, but now aligned with the ectopic spike. Note that, at the proximal location, the ectopic spike evoked a Ca^{2+} transient but not at the distal location; nevertheless, the oscillation in the Ca^{2+} fluorescence was reset to coincide with the next spike in the series.

proximately half that seen near body temperature, in agreement with previous work (Guatteo et al., 2005). However, application of isradipine (5 μM) for 10–15 min failed to significantly slow the discharge rate at 25°C (control median, 0.67 Hz; plus isradipine, 0.78 Hz; $n = 4$; $p > 0.05$) (supplemental Fig. S1, available at www.jneurosci.org as supplemental material). Again, this was not because isradipine had failed to antagonize L-type channels, because the SOPs were absent when the membrane patch was disrupted to monitor transmembrane voltage (supplemental Fig. S1, available at www.jneurosci.org as supplemental material). One interpretation of these results is that the dendrites or axon initial segment (AIS), which are sheared off during acute isolation, contribute to pacemaking, rendering it sensitive to antagonism of L-type Ca^{2+} channels. Underscoring the importance of these regions to the pacemaking process, SNc DA neurons in tissue slices also were insensitive to TRP channel antagonists 2-APB (20 μM; $n = 4$; $p > 0.05$) and SKF 96365 [1-2-(4-methoxyphenyl)-2-[3-(4-methoxyphenyl)propoxy]ethyl-1*H*-imidazole] (20 μM; $n = 4$; $p > 0.05$), in contrast to the situation reported in acutely isolated DA neurons (Kim et al., 2007).

Somatic and dendritic compartments are electrically coupled

The prevailing Ca^{2+} channel-dependent model of pacemaking hypothesizes that dendritic and somatic Ca^{2+} oscillations are

coupled, synchronizing the somatodendritic membrane potential and driving spike generation (Wilson and Callaway, 2000). A key feature of the coupled oscillator model is strong electrical coupling between somatic and dendritic compartments, leading to synchronization of the membrane potential. This means that oscillations in Ca^{2+} concentration should be phase locked in dendritic and somatic compartments. To test these two aspects of the model, line scans assessing changes in Ca^{2+} concentration were performed at both proximal and distal dendritic regions of SNc DA neurons during pacemaking; averages of the Ca^{2+}-induced fluorescence just before and after the spike were then calculated. In agreement with this aspect of the model, the proximal and distal dendritic Ca^{2+} signals were tightly phase locked in all neurons examined ($n = 4$), rising with the depolarization that preceded the spike and peaking just after the spike (Fig. 4*a*). Computer simulations with a single compartment model of an SNc DA neuron containing low-threshold $Ca_v1.3$ Ca^{2+} channels yielded a very similar relationship between intracellular Ca^{2+} concentration and membrane potential (Fig. 4*b*), arguing that the slow depolarization preceding the spike was driving Ca^{2+} channel opening throughout the dendritic tree.

Although the dendritic tree might be electrotonically compact for slowly changing signals, like those in the interspike period, there should be greater attenuation of more rapidly changing voltages unless there are active processes involved (Holmes and Rall, 1992). Previous work has shown that spikes originate in the AIS of SNc DA neurons and that, in the absence of pacemaking, these action potentials are actively propagated into distal dendritic regions (Häusser et al., 1995). However, action potential propagation is strongly influenced by even small changes in membrane potential (Gentet and Williams, 2007), making it uncertain whether there is back-propagation during pacemaking. If conducted into the dendrites, these spikes should reset dendritic oscillations that rely on voltage-dependent Ca^{2+} channels. To test this possibility, ectopic spikes were generated in the somatic region by a brief current pulse and the effects on somatic and dendritic oscillations monitored (Fig. 4*c*). In all of the neurons studied ($n = 4$), ectopic spikes occurring in the first half of the pacemaking cycle phase delayed the next spike, suggesting that the pacemaking mechanism had been reset (Fig. 4*d*). In some cells (like the one illustrated in Fig. 4), the spike only propagated into the proximal dendritic regions as judged by the change in Ca^{2+}-dependent fluorescence (Fig. 4*e*), suggesting that resetting the somatic component of the pacemaker was sufficient to reset the entire pacemaking process. These results are consistent with strong somatodendritic coupling posited in previous models but argue that the Na^+ channel-dependent spike itself is a key part of the pacemaking mechanism, not simply an epiphenomenon riding on top of the SOP, and that this proximally generated event determines pacemaking rate. This conclusion is consistent with the work presented above, showing that pacemaking continues unaltered in frequency or regularity in the absence of dendritic Ca^{2+} oscillations and the SOP.

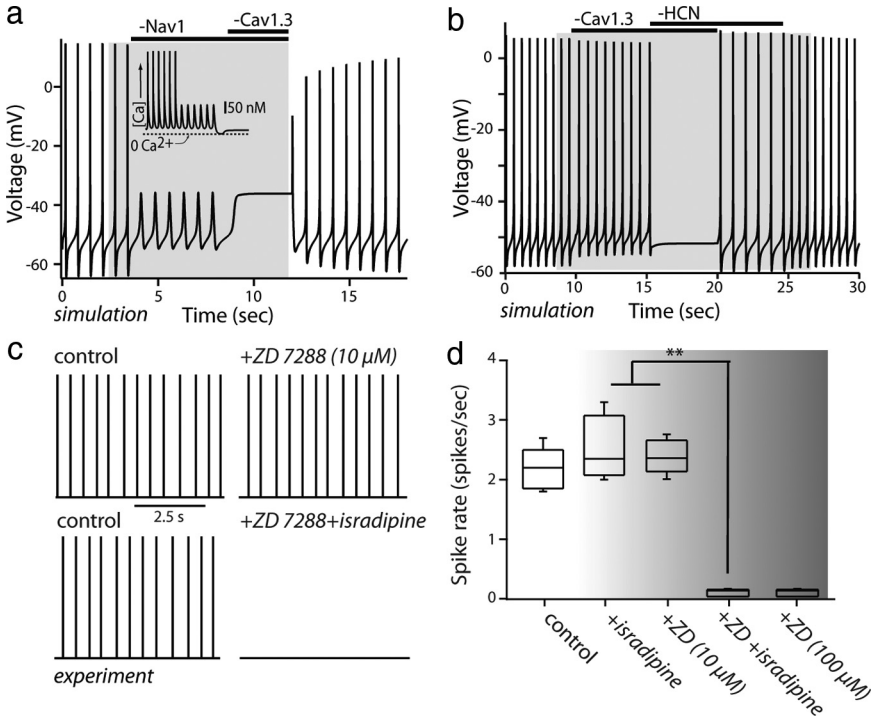

Figure 5. Simulations of pacemaking behavior and sensitivity to channel antagonism. ***a***, Voltage measurements from a single compartment simulation of an SNc DA neuron before and after removal of Na^+ channels, showing SOP-like behavior, and then after the additional removal of $Ca_v1.3$ Ca^{2+} channels, showing cessation of the SOP. Restoring the channels led to restoration of pacemaking. Inset is intracellular Ca^{2+} concentrations in the model before and after removal of Na^+ channels. Timing of the changes is shown in the bars at the top. ***b***, Voltage measurements of a simulation in which there was successive removal of first $Ca_v1.3$ and then combined removal of HCN and $Ca_v1.3$ channels. Note that pacemaking stopped only with the removal of both channels. ***c***, Digitized cell-attached patch recordings before and after application of ZD 7288 (10 μM) showing no significant change in discharge rate (see summary in ***d***). At the bottom, digitized cell-attached patch recordings before and after application of ZD 7288 (10 μM) and isradipine (5 μM) showing silencing of the cell. ***d***, Summary of experiments as in ***c***. The fall in discharge rates with coapplication of ZD 7288 (10 μM) and isradipine (5 μM) or with application of high concentrations of ZD 7288 (100 μM) alone was significant (**$p < 0.01$). Sample sizes were control ($n = 6$), isradipine (5 μM; $n = 7$), low ZD 7288 (10 μM; $n = 8$), low isradipine plus low ZD 7288 ($n = 5$), and high ZD 7288 (100 μM; $n = 4$).

A computational model accounts for the insensitivity to DHPs

In an attempt to gain a better conceptual foothold on the mechanisms controlling pacemaking, a computational model was created using NEURON. The model consisted of a single "somatic" compartment; biophysically accurate models of channels thought to govern pacemaking were incorporated at densities resembling those seen experimentally (see Materials and Methods). The model generated regular, autonomous spiking at 1–2 Hz (Fig. 5*a*). As observed experimentally (Puopolo et al., 2007), the $Ca_v1.3$ Ca^{2+} current was significantly larger than the Na_v1 Na^+ current in the interspike interval (supplemental Fig. S2, available at www.jneurosci.org as supplemental material); however, both currents were significantly smaller than those generated by "leak" channels, as in previous simulations (Amini et al., 1999). Reducing the Na_v1 channel density to zero prevented spiking but did not stop subthreshold oscillations, but subsequent block of $Ca_v1.3$ channels did, stabilizing the membrane potential near −40 mV.

Having verified that the basic behavior of the model resembled that seen experimentally, the interaction between $Ca_v1.3$

channels and other cationic channels in regulating pacemaking was explored. Eliminating $Ca_v1.3$ channels had little effect on pacemaking rate, despite clear effects on the voltage trajectory (Fig. 5*b*). Similarly, completely eliminating HCN channels had little effect on pacemaking rate. In both cases, the loss of inward current was compensated for by alterations in other conductances (supplemental Fig. S2, available at www.jneurosci.org as supplemental material). The combined removal of HCN and $Ca_v1.3$ channels, however, stopped spiking (Fig. 5*b*).

These results suggest that pacemaking is a robust, cooperative process, capable of withstanding perturbations in the availability of any one channel. To test this idea, recordings were made from SNc DA neurons, and combinations of channels were antagonized pharmacologically. Selective block of HCN channels with saturating concentrations of ZD 7288 (10 μM) had little or no effect on pacemaking rate (Fig. 5*c*,*d*). However, as predicted by the simulations, blocking HCN channels rendered pacemaking sensitive to antagonism of L-type Ca^{2+} channels, because application of isradipine (5 μM) in the presence of ZD 7288 (10 μM) silenced every SNc DA neuron tested ($n = 5$) (Fig. 5*c*,*d*). It is worth noting that higher concentrations of ZD 7288 (50–100 μM) antagonized non-HCN channels (Zolles et al., 2006) and stopped pacemaking on their own (Fig. 5*d*).

High concentrations of DHPs stop pacemaking by affecting other channel types

Why do high concentrations of DHPs, like isradipine, reliably slow or stop pacemaking in SNc DA neurons (Nedergaard et al., 1993; Mercuri et al., 1994; Ping and Shepard, 1996; Chan et al., 2007)? The work presented thus far argues that significant slowing or silencing is not attributable to antagonism of $Ca_v1.3$ Ca^{2+} channels and must be attributable to reductions in other inward currents that help support pacemaking. There are three potential targets: Na_v1 Na^+, HCN, and cation leak channels. Point-clamp experiments using slow, depolarizing voltage ramps revealed that 20 μM isradipine modestly but consistently reduced peak Na^+ currents in SNc DA neurons (median reduction, 27%; $n = 4$; $p < 0.05$). In contrast, isradipine did not reduce the amplitude of the voltage sag produced by hyperpolarizing current steps (median reduction, 0.04%; $n = 6$; $p > 0.05$). However, input conductance measured by small hyperpolarizing steps from −60 mV was significantly reduced by isradipine, suggesting that cationic leak channels were being partially blocked (median reduction, 31%; $n = 9$; $p < 0.05$). Reducing Na^+ and leak channel density together by 20% consistently silenced pacemaking in the model, making this explanation plausible (Fig. 6*a*).

With sustained application of silencing concentrations of isradipine, pacemaking restarts after several hours (Chan et al., 2007). It could be restarted immediately by application of K_v1 channel antagonists (Fig. 6*b*,*c*), suggesting that the delayed restarting seen previously depends on functional downregulation of these channels. The model captured this recovery, because the silencing produced by partial block of Na^+ and leak channels was reversed by block of K_v1 channels (Fig. 6*a*). More importantly, this result reinforces the proposition that pacemaking reflects the interaction of a network of ion channels that is capable of withstanding perturbations in individual components.

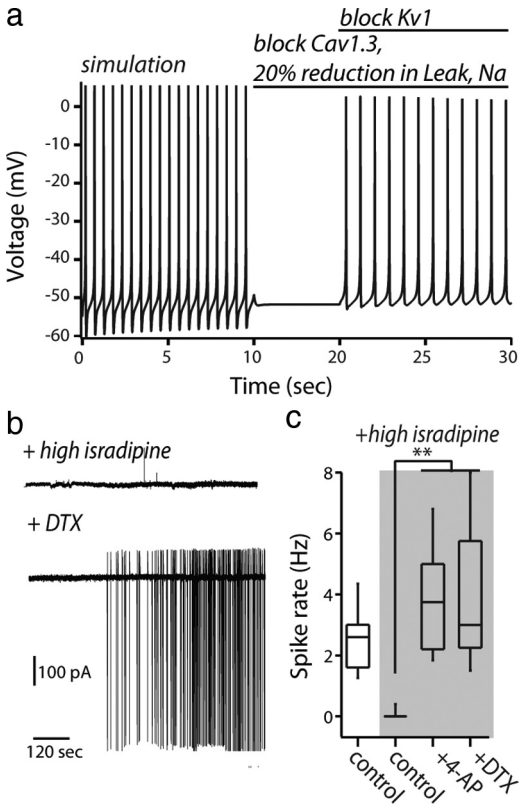

Figure 6. Pacemaking in DA neurons silenced with high DHP is restored by blocking K_v1 channels. ***a***, NEURON simulation model of pacemaking firing previous and after blockade of $Ca_v1.3$, 20% reduction in sodium current, and 20% reduction in leak currents. Combined partial blockade of these inward currents silenced pacemaking as in the experimental conditions described below (***b***, ***c***). Spiking activity was restored on blockade of K_v1 channels. ***b***, Cell-attached patch recording from an SNc DA neuron that had been silenced by isradipine (20 μM) and then restarted by bath application of α-dendrotoxin (DTX; 100 nM). ***c***, Summary of similar experiments showing discharge rates in control ($n = 8$), isradipine exposed ($n = 6$), and then cells exposed to either α-dendrotoxin (100 nM; $n = 6$) or 4-aminopyridine (100 μM; $n = 6$); the change in discharge rate after exposure to either toxin was significant (**$p < 0.01$) when compared with the isradipine-induced silenced state.

Discussion

Our principal conclusion is that, although L-type Ca^{2+} channels contribute to the oscillatory behavior of SNc DA neurons, they are not necessary for autonomous pacemaking (Nedergaard et al., 1993; Mercuri et al., 1994; Wilson and Callaway, 2000; Puopolo et al., 2007). Our work shows that there is an interactive network of ion channels in SNc DA neurons that is capable of sustaining pacemaking even when parts of it, like L-type Ca^{2+} channels, are antagonized. This finding adds another dimension to an array of other observations showing that the rate of autonomous spiking in SNc DA neurons is insensitive to a variety of extrinsic and intrinsic perturbations (Paladini et al., 2003; Chan et al., 2007), a testament to the importance of pacemaking in the maintenance of DA in target structures involved in movement, learning, and cognition.

Pacemaking in SNc DA neurons is robust

The view that somatodendritic L-type Ca^{2+} channels contribute to pacemaking in SNc DA neurons has a long history. Initially, it was found that, in the presence of the Na^+ channel blocker TTX, the membrane potential of SNc DA neurons continued to oscillate at near the pacemaking frequency (Yung et al., 1991; Nedergaard et al., 1993). This SOP was sensitive to blockade of Ca^{2+} channels and, more importantly, to DHPs that antagonize L-type Ca^{2+} channels (Nedergaard et al., 1993; Mercuri et al., 1994). The hyperpolarizing phase of this oscillation is brought about by activation of Ca^{2+}-activated SK K^+ channels (Ping and Shepard, 1996). The ability of DHPs to suppress the SOPs has been repeated by several

groups (Nedergaard et al., 1993; Chan et al., 2007). It was natural to infer from the temporal similarity of the oscillatory potential and pacemaking that the two processes were causally linked. This inference was supported by the ability of DHPs to slow or stop the regular spiking of SNc DA neurons (Nedergaard et al., 1993; Mercuri et al., 1994). However, in previous experiments, silencing typically required DHP concentrations in the low micromolar range, several orders of magnitude above the K_D of DHPs for the $Ca_v1.3$ L-type Ca^{2+} channels that drive the SOP.

Our work argues that the ability of DHPs at these high concentrations to slow or stop pacemaking has little to do with L-type Ca^{2+} channels. There are five key pieces of experimental evidence on this point. First, Ca^{2+} imaging studies showed that intracellular fluctuations in Ca^{2+} concentration attributable to opening of L-type Ca^{2+} channels were significantly attenuated or eliminated by application of the DHP isradipine at concentrations that did not alter pacemaking rate. Second, concentrations of isradipine that blocked SOPs did not alter pacemaking rate. Third, SOPs were less regular and often slower than pacemaking. Fourth, chelation of intracellular Ca^{2+} did not stop or slow pacemaking but rather accelerated it. Last, the ability of an ectopic somatic spike to reset the Ca^{2+} oscillation throughout the dendritic tree, even when there was no evidence that the spike invaded the distal dendrites, argues that Na^+-dependent spikes originating in the AIS (Häusser et al., 1995) pace the somatodendritic oscillations, determining their rate and regularity, not the other way around.

Simulations that incorporated realistic descriptions of the ion channels known to participate in pacemaking provided an explanation for much of the experimental data. Not only did the model generate autonomous spiking of the right rate and regularity, it also produced SOPs when Na^+ channels were blocked that strongly resembled those seen experimentally. The model also sustained pacemaking in the absence of L-type Ca^{2+} channels, showing how the compensatory changes in other conductances served to maintain the discharge rate. Thus, the channels expressed by SNc DA neurons form an interactive network that is capable of maintaining pacemaking in the face of perturbations in the channel availability. This level of robustness should provide a means of withstanding fluctuations in channel availability as a consequence of neuromodulatory challenge or synaptically driven activity.

That said, the robustness of the model and real SNc DA neurons was limited. Combined antagonism of $Ca_v1.3$ and HCN channels stopped pacemaking, although antagonism of either alone had little or no effect, just as observed experimentally. The sensitivity of SNc DA neurons to the combined disruption of a mixed population of ion channels helps explain the effects of high DHP concentrations on pacemaking. At DHP concentrations that consistently induced silencing, isradipine reduced not only L-type Ca^{2+} channel currents but Na^+ channel currents and leak channel currents as well. Simulations showed how this combined antagonism could account for cessation of pacemaking. This also means that experimental interventions that compromise the pacemaking mechanism could lead to a spurious elevation in the sensitivity to DHPs. Our assessment of DHP sensitivity relied primarily on cell-attached patch recordings that did not alter the intracellular environment the way whole-cell or sharp electrode recordings can. In cell-attached patch recordings, there was not a graded slowing of pacemaking with increasing DHP concentration; rather, at a well defined time point after bath application, cells continued at a normal rate, became irregular, or stopped entirely (as also described by Nedergaard et al., 1993). In our hands, this transition occurred at DHP concentrations at which other channels besides L-type Ca^{2+} channels were being blocked. This was also true in our simulations. As a consequence, the slowing of pacemaking at lower DHP concentrations described by Mercuri et al. (1994) or anecdotally by Nedergaard et al. (1993) in brain slices can only be explained (within our framework) by positing that either (1) their sharp electrode recordings disrupted the capacity of these collateral ionic mechanisms to compensate for the loss of L-type channels or (2) because of lipid phase partitioning [DHP partition coefficients >1000 (Herbette et al., 1989)] and extended drug exposure, DHP concentration in the membrane had risen to levels at which non-L-type channels were being affected, despite the fact that bath concentrations were below 10 μM. The difficulty of this pharmacokinetic problem was one of the primary motivations for our use of Ca^{2+} imaging to monitor fluctuations in dendritic Ca^{2+} concentration during drug application, giving us a much more direct way of monitoring effective membrane concentrations of bath-applied DHPs. Although potentially an issue in brain slices, pharmacokinetics is not a major concern with acutely isolated neurons, but there are other issues. In their biophysical study, Puopolo et al. (2007) reported that low micromolar, selective concentrations of nimodipine had variable effects on pacemaking of acutely isolated DA neurons recorded with whole-cell methods, sometimes slowing or stopping pacemaking, sometimes having no effect. This variability is most readily attributed to the one variable that is poorly controlled with this approach, the degree to which dendritic and axonal arbors are truncated. Although not necessary, these are regions that very likely contribute in a material way to the robustness of pacemaking (Tepper et al., 1987; Grace and Onn, 1989; Häusser et al., 1995; Amini et al., 1999; Wilson and Callaway, 2000).

What does this mean for a potential neuroprotective therapy in PD?

The robustness of pacemaking in SNc DA neurons has implications for neuroprotective therapies. Ca^{2+} entry through L-type Ca^{2+} channels renders SNc DA neurons vulnerable to a range of toxins used to create animal models of PD (Chan et al., 2007). Moreover, DHP use in humans is associated with a decreased incidence of PD (Becker et al., 2008). Isradipine is now being tested in clinical trials for its ability to modify PD progression. At the doses to be used in this study, isradipine achieves stable serum concentrations of ~2 ng/ml, which is close to the serum concentration that is neuroprotective in animal models of PD (our unpublished observations). If we assume that brain and serum concentrations are similar (Kupsch et al., 1996), isradipine should be ~5 nM in the extracellular space bathing SNc DA neurons, which should antagonize between 70 and 80% of their $Ca_v1.3$ Ca^{2+} channels, assuming a modal membrane potential of −50 mV (Bean, 1984; Sinnegger-Brauns et al., 2009). Our results show that the neuroprotection afforded by this antagonism should not come at the cost of a reduction in basal pacemaking rate in SNc DA neurons.

References

Albin RL, Young AB, Penney JB (1989) The functional anatomy of basal ganglia disorders. Trends Neurosci 12:366–375.

Amini B, Clark JW Jr, Canavier CC (1999) Calcium dynamics underlying pacemaker-like and burst firing oscillations in midbrain dopaminergic neurons: a computational study. J Neurophysiol 82:2249–2261.

Bean BP (1984) Nitrendipine block of cardiac calcium channels: high-affinity binding to the inactivated state. Proc Natl Acad Sci U S A 81:6388–6392.

Becker C, Jick SS, Meier CR (2008) Use of antihypertensives and the risk of Parkinson disease. Neurology 70:1438–1444.

Chan CS, Guzman JN, Ilijic E, Mercer JN, Rick C, Tkatch T, Meredith GE, Surmeier DJ (2007) "Rejuvenation" protects neurons in mouse models of Parkinson's disease. Nature 447:1081–1086.

Cohen MX, Frank MJ (2009) Neurocomputational models of basal ganglia function in learning, memory and choice. Behav Brain Res 199:141–156.

Gentet LJ, Williams SR (2007) Dopamine gates action potential backpropagation in midbrain dopaminergic neurons. J Neurosci 27:1892–1901.

Gonon F, Bloch B (1998) Kinetics and geometry of the excitatory dopaminergic transmission in the rat striatum in vivo. Adv Pharmacol 42:140–144.

Grace AA, Bunney BS (1984) The control of firing pattern in nigral dopamine neurons: single spike firing. J Neurosci 4:2866–2876.

Grace AA, Onn SP (1989) Morphology and electrophysiological properties of immunocytochemically identified rat dopamine neurons recorded *in vitro*. J Neurosci 9:3463–3481.

Guatteo E, Chung KK, Bowala TK, Bernardi G, Mercuri NB, Lipski J (2005) Temperature sensitivity of dopaminergic neurons of the substantia nigra pars compacta: involvement of transient receptor potential channels. J Neurophysiol 94:3069–3080.

Häusser M, Stuart G, Racca C, Sakmann B (1995) Axonal initiation and active dendritic propagation of action potentials in substantia nigra neurons. Neuron 15:637–647.

Herbette LG, Vant Erve YM, Rhodes DG (1989) Interaction of 1,4 dihydropyridine calcium channel antagonists with biological membranes: lipid bilayer partitioning could occur before drug binding to receptors. J Mol Cell Cardiol 21:187–201.

Hines ML, Carnevale NT (2001) NEURON: a tool for neuroscientists. Neuroscientist 7:123–135.

Holmes WR, Rall W (1992) Estimating the electrotonic structure of neurons with compartmental models. J Neurophysiol 68:1438–1452.

Kim SH, Choi YM, Jang JY, Chung S, Kang YK, Park MK (2007) Nonselective cation channels are essential for maintaining intracellular Ca^{2+} levels and spontaneous firing activity in the midbrain dopamine neurons. Pflugers Arch 455:309–321.

Koschak A, Reimer D, Huber I, Grabner M, Glossmann H, Engel J, Striessnig J (2001) alpha 1D (Cav1.3) subunits can form l-type Ca^{2+} channels activating at negative voltages. J Biol Chem 276:22100–22106.

Kupsch A, Sautter J, Schwarz J, Riederer P, Gerlach M, Oertel WH (1996) 1-Methyl-4-phenyl-1,2,3,6-tetrahydropyridine-induced neurotoxicity in non-human primates is antagonized by pretreatment with nimodipine at the nigral, but not at the striatal level. Brain Res 741:185–196.

Lipkind GM, Fozzard HA (2003) Molecular modeling of interactions of dihydropyridines and phenylalkylamines with the inner pore of the L-type Ca^{2+} channel. Mol Pharmacol 63:499–511.

Mercer JN, Chan CS, Tkatch T, Held J, Surmeier DJ (2007) $Na_v1.6$ sodium channels are critical to pacemaking and fast spiking in globus pallidus neurons. J Neurosci 27:13552–13566.

Mercuri NB, Bonci A, Calabresi P, Stratta F, Stefani A, Bernardi G (1994) Effects of dihydropyridine calcium antagonists on rat midbrain dopaminergic neurones. Br J Pharmacol 113:831–838.

Nedergaard S, Flatman JA, Engberg I (1993) Nifedipine- and omega-conotoxin-sensitive Ca^{2+} conductances in guinea-pig substantia nigra pars compacta neurones. J Physiol 466:727–747.

Paladini CA, Robinson S, Morikawa H, Williams JT, Palmiter RD (2003) Dopamine controls the firing pattern of dopamine neurons via a network feedback mechanism. Proc Natl Acad Sci U S A 100:2866–2871.

Ping HX, Shepard PD (1996) Apamin-sensitive Ca^{2+}-activated K^+ channels regulate pacemaker activity in nigral dopamine neurons. Neuroreport 7:809–814.

Puopolo M, Raviola E, Bean BP (2007) Roles of subthreshold calcium current and sodium current in spontaneous firing of mouse midbrain dopamine neurons. J Neurosci 27:645–656.

Schultz W (2007) Multiple dopamine functions at different time courses. Annu Rev Neurosci 30:259–288.

Sinnegger-Brauns MJ, Huber IG, Koschak A, Wild C, Obermair GJ, Einzinger U, Hoda JC, Sartori SB, Striessnig J (2009) Expression and 1,4-dihydropyridine-binding properties of brain L-type calcium channel isoforms. Mol Pharmacol 75:407–414.

Tepper JM, Sawyer SF, Groves PM (1987) Electrophysiologically identified nigral dopaminergic neurons intracellularly labeled with HRP: light-microscopic analysis. J Neurosci 7:2794–2806.

Tepper JM, Paladini CA, Celada P (1998) GABAergic control of the firing pattern of substantia nigra dopaminergic neurons. Adv Pharmacol 42:694–699.

Wilson CJ, Callaway JC (2000) Coupled oscillator model of the dopaminergic neuron of the substantia nigra. J Neurophysiol 83:3084–3100.

Yin HH, Ostlund SB, Balleine BW (2008) Reward-guided learning beyond dopamine in the nucleus accumbens: the integrative functions of cortico-basal ganglia networks. Eur J Neurosci 28:1437–1448.

Yung WH, Häusser MA, Jack JJ (1991) Electrophysiology of dopaminergic and non-dopaminergic neurones of the guinea-pig substantia nigra pars compacta in vitro. J Physiol 436:643–667.

Zolles G, Klöcker N, Wenzel D, Weisser-Thomas J, Fleischmann BK, Roeper J, Fakler B (2006) Pacemaking by HCN channels requires interaction with phosphoinositides. Neuron 52:1027–1036.